| Title | Nanotubes of core/shell Cu/Cu2O as anode materials for Li-ion rechargeable batteries |
|---|---|
| Authors | Hasan, Maksudul;Chowdhury, Tamjid;Rohan, James F. |
| Publication date | 2010-06 |
| Original Citation | HASAN, M., CHOWDHURY, T. & ROHAN, J. F. 2010. Nanotubes of Core/Shell Cu/Cu2O as Anode Materials for Li-Ion Rechargeable Batteries. Journal of The Electrochemical Society, 157, A682-A688. doi: 10.1149/1.3364794 |
| Type of publication | Article (peer-reviewed) |
| Link to publisher's version | http://jes.ecsdl.org/content/157/6/A682.abstract - 10.1149/1.3364794 |
| Rights | © The Electrochemical Society, Inc. 2010. All rights reserved. Except as provided under U.S. copyright law, this work may not be reproduced, resold, distributed, or modified without the express permission of The Electrochemical Society (ECS). The archival version of this work was published in HASAN, M., CHOWDHURY, T. & ROHAN, J. F. 2010. Nanotubes of Core/Shell Cu/Cu2O as Anode Materials for Li-Ion Rechargeable Batteries. Journal of The Electrochemical Society, 157, A682-A688. doi: 10.1149/1.3364794 |
| Download date | 2024-05-07 11:12:57 |
| Item downloaded from | https://hdl.handle.net/10468/1347 |

**Nanotubes of core/shell Cu/Cu$_2$O as anode materials for Li-ion rechargeable batteries.**

**Maksudul Hasan, Tamjid Chowdhury and James F. Rohan\***

Tyndall National Institute, University College Cork, Lee Maltings, Cork, Ireland.

\* Corresponding author. Tel.: +353 21 4904224; fax: +353 21 4270271.

*E-mail address*: james.rohan@tyndall.ie (James F. Rohan)

**Abstract.**

A direct electrodeposition technique for Cu nanotube array fabrication and subsequent conversion of the deposited Cu into $Cu_2O$ has been developed. The $Cu_2O$ nanotube arrays have shown high capacity, cyclability and rate capability. The cycling performance of the $Cu_2O$ nanotubes show a high level of structural integrity with capacity retention even after 94 cycles when cycled at 1C to 3C rates. The enhanced electrochemical performance of the $Cu_2O$ nanotubes comes from high surface area, electrolyte access, high electrical conductivity of Cu core support and structural integrity of the oxide shell active material.

**Introduction**

One dimensional (1D) nanostructures have recently attracted much attention for potential applications in nanoscale energy storage/conversion devices [1-3] due to their unique physical properties that differ from the bulk materials. 1D nanostructures provide additional electrode surface area, to facilitate $Li^+$ insertion/extraction and short path lengths for electronic and $Li^+$ transport and thus the possibility of higher charge/discharge rates [4]. Recently, metal oxides of Fe, Co and Cu have been described as anode materials for Li-ion batteries based on a novel reaction mechanism proposed by Tarascon et al [5]. More recently, they demonstrated the idea of the so called "conversion reactions" for 1D $Fe_3O_4$ nanorod structures [6]. The reaction mechanism involves the compositional transformation of metal oxides to metal nanodomains dispersed in $Li_2O$ during the charging process which regain the original composition during the discharge process. The reaction mechanism differs from the classical $Li^+$ insertion/de-insertion. High rate capability (for example, 80% capacity retention at 8 C rates) was reported [6] using these nanorod arrays. Mesoporous $Co_3O_4$ nanorods of the same "conversion reactions" family have been synthesised by an ammonia-evaporation-induced method on Si wafer, glass slide, Cu or Ti foil, and polystyrene substrates [7]. This template-free method permits the growth of large area nanorod arrays on various substrates. $Cu_2O$ is also a "conversion reaction" oxide family member with demonstrated high capacity [8]. $Cu_2O$ nanowires have been fabricated in anodised alumina oxide (AAO) templates by electrodeposition from a copper acetate/lactate bath with Cu as co-deposit [9]. The variation of local pH at the electrode surface during the deposition process results in the spontaneous potential oscillation and a $Cu/Cu_2O$ composite deposit. However, the low efficiency of the bath has restricted its applications. Yang et al. oxidised $Cu_2S$ nanowires under $O_2$ at elevated

temperature and observed the formation of polycrystalline nanowires containing both Cu and $Cu_2O$ [10].

In this paper, we will report a novel fabrication route to Cu nanotubes based on the direct electrodeposition of Cu in the pores of an alumina template from an additive containing $CuSO_4$ bath and the controlled conversion of the deposited Cu into $Cu_2O$. The novelty of the method is the simplicity and control in producing a very high quality $Cu/Cu_2O$ nanotube array. Cu nanotubes have been grown previously in polycarbonate templates through a chemical reduction method for use as additives in the negative electrode of Ni-MH batteries [11]. Another method involved sequential high temperature processing steps to achieve template assisted nanotube deposition [12]. We will present the mechanism for Cu nanotube growth and conversion to $Cu_2O$ for use as a lithium battery anode. Characterisation of the materials by XRD, electrochemical performance and microstructure analysis by SEM is utilised to correlate with the Li cycling performance.

**Experimental**

Cu nanotubes were electrodeposited in AAO (Anodisc membranes, Whatman, 19.5 mm in diameter excluding of the polypropylene supporting ring, 60 μm thick and $10^9$ pores per $cm^2$). The pore diameter was 250 to 300 nm. The complete fabrication process of $Cu_2O$ nanotubes is illustrated in Fig. 1. A 500 nm thin layer of Ni conducting layer was deposited onto one side of AAO template by e-beam evaporation (Temescal FC-2000). The electrodeposition was carried out in a 0.24 M $CuSO_4$ (Fisher Scientific analytical reagent grade) and 1.8 M $H_2SO_4$ (Air products 96%) bath at room temperature with slow

4

stirring of the solution. The additives used in the bath were polyethylene glycol (PEG) (300 ppm) (SigmaUltra, mol. wt. 3350, powder) and $Cl^-$ (50 ppm) as NaCl (BDH, analytical reagent grade). A constant current 40 mA was applied for Cu nanotubes electrodeposition using a potentiostat CH Instruments 660C in a two electrode set up with Cu foil as the anode and the Ni substrate at the base of the pores of the AAO as the cathode. The AAO template was mounted vertically in the cell facing the anode with the Ni seed layer on the opposite side open to the solution. The spacing between the anode and cathode was maintained at 1 cm. A Cu wire was connected to the Ni conducting side of the template by Ag conductive paint (Radionics Ltd. Ireland). The deposition rate was approximately 0.22 μm per minute. After Cu deposition the aluminium oxide template was dissolved in 0.75 M NaOH (Sigma Aldrich) solution for 50 min, washed with DI water and dried in air.

The electrodeposited Cu was converted to $Cu_2O$ by oxygen plasma treatment (March Plasmod GCM 200) at 250 watts. The Li capacity test of $Cu_2O$ nanotubes was performed by cyclic voltammetry and constant current experiments using a CH Instruments 660C potentiostat and a three electrode set-up. The active weight of the of $Cu_2O$ nanotubes was estimated from the height, diameter (calculated from conversion rate plots in the results section for Cu to $Cu_2O$) and number of nanowires ($10^9$ pores/$cm^2$ in Whatman AAO membranes) in a 19.5 $cm^2$ AAO template, and assuming the $Cu_2O$ density of 6.09 g/$cm^3$, The $Cu_2O$ nanotubes arrays as obtained were mounted vertically in a Pyrex glass cell filled with electrolyte, in which $Cu_2O$ nanotubes assembly was served as working electrode and 0.25 mm lithium foil (Sigma-Aldrich) as counter and reference electrodes. The electrolyte was 1M $LiPF_6$ in ethylene carbonate (EC)/diethyl carbonate (DEC) (1:1, in volume) (Sigma-Aldrich). Lithium foil of 0.25 mm thickness (Sigma-Aldrich) served

as counter and reference electrodes. The cell was assembled in an MBraun argon-filled glove box where $O_2$ and $H_2O$ were maintained at or leow a 0.1 ppm level. The capacity values were measured by calculating the total Coulombic charge during $Li^+$ ions insertion and extraction for the discharge and charge curves, respectively.

The materials were characterised by X-ray powder diffraction (Phillips PW3710-MPD with Cu K$\alpha$ radiation, l = 1.54056 Å, at 40 kV (35 mA) and data was analysed using Philips X'pert XRD software). The deposit microstructure was analysed by scanning electron microscopy (SEM) (FEI Nova 630 Nano-SEM at 15 kV).

**Results and Discussion**

Well ordered and homogeneous Cu nanotubes were obtained using a template mediated electrodeposition technique from a $CuSO_4/H_2SO_4$ bath with the additives (PEG and Cl$^-$) at room temperature [13]. Only when both PEG and Cl$^-$ additives are added in the bath does the growth mechanism lead to Cu nanotubes rather than solid metallic nanowires, Figs. 2(a) and (b). The electrodeposited Cu nanotubes are converted to $Cu_2O$ by oxygen plasma treatment. This plasma ash technique is commonly used to remove organic residues after the processing in the semiconductor or packaging industries. The oxygen plasma technique was found to be efficient in the conversion of the deposited Cu in nanotube format to $Cu_2O$ oxides. The microstructure of the $Cu_2O$ nanotube arrays studied by SEM is shown in Figs. 3 (a) and (b).

XRD analysis of the Cu nanotubes prior to conversion to the oxide shows polycrystalline phases of 100, 200 and 220 orientation in Fig. 4(a). The oxidised nanotubes XRD data

6

(Fig. 4(b)) shows typical $Cu_2O$ phases of 111, 200, 211, 220, 311 and 222 in addition to the non-oxidised Cu metal phases. The polycrystalline nanotubes containing both $Cu_2O$ and Cu phases clearly indicates that the metallic Cu tubes have not been completely converted to oxides during the 4.5 minutes plasma treatment at 250 W. The oxidation time at a fixed power (250 W) was varied to achieve a minimum metallic tube wall thickness as the inner core support of the outer shell oxide layers. The conversion rates of Cu thin film and Cu nanotubes to $Cu_2O$ are shown in Fig. 5. The electrodeposited Cu thin film and Cu nanotubes of 3 $cm^2$ area and 20 μm long nanotubes were oxidised for the times shown. The formed oxide layers were chemically removed in a commercial oxide removal solution (Schloetter S20 - sulphuric acid based). The weight loss due to the oxide layer removal in this solution (Mettler Toledo XS105, repeatability (SD) = 0.02 mg) is plotted against the oxidation time in Fig. 5(a), which gives the conversion rate plot. The $Cu_2O$ conversation rate is correlated with the wall thickness of Cu metallic tubes as shown in Fig. 5(b) e.g., for 4.1 mins plasma treatment at the specified power of 250 W it is estimated to be 30 nm based on the weight loss on removing the oxide and assuming the $Cu_2O$ density of 6.09 $g/cm^3$. The thickness of the $Cu_2O$ is assumed to be 15 nm on both inner and outer nanotube walls and the remaining un-oxidised Cu nanotube support is approximately 45 nm, (given an outer tube diameter of 300 nm and inner diameter 150 nm. SEM images of the Cu nanotubes as deposited, after oxygen plasma treatment and after oxide removal are shown in figures 6 (a to c) respectively. The  thinned Cu core substrate after the process of oxide formation and removal is seen by comparing Figs 6(a) and 6(c).

The electrochemical performance of the $Cu_2O$ nanotubes was studied by cyclic voltammetry. Fig. 7(a) shows the first 20 cycles for $Cu_2O$ nanotubes with low oxide

content (~ 8 nm, or 2.32 mg / 3 cm$^2$, from oxygen plasma treatment for 1 min) at a sweep rate of 0.5 mV/s. In the first cycle, there is one broad cathodic peak located at 1.10 V and a small shoulder at 0.7 V, while in the following cycles three distinct cathodic reactions are observed at 1.55, 0.7 and approaching 0 V respectively. The peak at 1.10 V can be assigned to the Li$^+$ insertion reaction into Cu$_2$O and irreversible electrolyte reaction products that are not present in the second or subsequent cycles. The three regions in the following cycles are attributed to the Li$^+$ insertion reaction into Cu$_2$O crystallites [14-15]. The potential of the Li$^+$ insertion reactions and the formation of the protective interphase layer in the first cycle are so close that they appear as a broad single peak. Meanwhile, one extended oxidation wave starting at 0.2 V up to a peak at 2.55 V corresponds to Li$^+$ de-insertion from the crystal lattice of Cu$_2$O nanotubes. It also can be seen from Fig. 7(a) that the potential of the Li$^+$ insertion reaction increases in the cycles following the first.

Cu$_2$O is among a group of metal oxides that demonstrate a novel reactivity mechanism which differs from the classical Li$^+$ insertion or de-insertion and involves the formation and decomposition of Li$_2$O [5]. Cu$_2$O transfers two electrons in the electrochemical reaction (with a theoretical capacity of 375 mAhg$^{-1}$) and such reduction enables the conversion into nanocomposite materials consisting of nanometre scale Cu metallic clusters in the range 1 to 5 nanometres as reported by Tarascon et al. dispersed in an amorphous Li$_2$O matrix, according to the following redox reaction [5].

$$Cu_2O + 2Li^+ + 2e^- \rightarrow 2Cu + Li_2O \qquad [1]$$

The SEM image (Fig. 3a) shows that oxide morphology is not uniform along the nanotubes. At the beginning of the reaction, the particle size of Cu$_2$O on the nanotubes is

8

inhomogeneous. The SEM images of Fig. 11 (a) and (b) indicate the formation of homogeneous nanosized $Cu_2O$ crystallites during the conversion reaction in Li cycling. The formation of homogeneous $Cu_2O$ crystallite morphology leads to uniform reactivity towards Li and the consequent dispersion of nanometre scale Cu metallic clusters in the amorphous $Li_2O$ improves the reversibility of $Li_2O$ back to Li in the charge cycle due to interconnected network between the $Li_2O$ particles. Therefore, the potential of the $Li^+$ insertion reaction into $Cu_2O$ increases after the first cycle and remains constant in all the following cycles showing balanced discharge-charge behaviour. The complete overlapping of the cyclic voltammograms in continueous cycling indicates the reversibilty of $Li^+$ insertion and de-insertion reactions in $Cu_2O$ due to the homogeneous crystallites on the nanotube supports. Fig. 7(b) is a discharge-charge curve of $Li^+$ in $Cu_2O$ nanotubes by cyclic voltammetry showing the specifice Li storage capacity is still around 375 mAhg$^{-1}$ after 30 cycles with no significant deterioration. Additionally, the increased surface area of $Cu_2O$ nanotubes due to the inner wall and the open tube end provides electrolyte access and support for fast ionic mass transport to the remote electrode area. The capacity retention of the self-supported $Cu_2O$ nanotube electrodes may be attributed to the short $Li^+$ and $e^-$ transport length, easy penetration of electrolyte into the pores and increased electrolytic contact area. The irreversible capacity loss in the first cycle is caused by irreversible electrolyte reactions at the $Cu_2O$ lattice surface, which hinders lithium ion movement to the anode [16-17]. These irreversible reactions are significant in nano-architectured electrodes because of the large surface and interface areas [18] but their formation decreases with cycling [19]. The irreversible capacity loss in the first cycle is also partly associated with the irreversible conversion reaction of $Li_2O$ due to lack of interconnected network formed between $Li_2O$ particles by nanosized Cu metallic

clusters. In this work the loss is apparent only on the first cycle and there are no additional irreversible peaks in the cathodic sweep.

In another experiment thicker $Cu_2O$ nanotubes were formed by oxygen plasma treatment for 4.5 min and according to the conversion correlation curve (Fig. 5(b)), about 34 nm of the solid Cu is converted to equilvalent $Cu_2O$. Fig. 8(a) shows the first three voltammograms of the $Cu_2O$ nanotubes recorded at a sweep rate of 0.5 mV/s. These curves show the same characteristics but higher current density (1.5 mA/cm$^2$) as seen for low content $Cu_2O$ electrodes at the same sweep rate. When the sweep rate is increased to 2 mV/s or 5 mV/s the current density increases but the shape of cyclic voltammograms is altered both in the cathodic or anodic regions, Fig. 8(b). At the higher sweep rate the cathodic peaks at 0.7 V and 1.15 V are a single wave until sweep reversal at 0 V while in the anodic region an oxidation peak is generated in the range of 0.5-1.0 V in addition to the peak at 2.55 V. The capacities in the potential range are the same as those recorded at slower sweep rates. Additionally, the polycrystalline $Cu_2O$ particles converted to homogeneous nanoparticulates with cycling may possess additional crystalline imperfections and grain boundary sites for hosting Li$^+$ ions. The charge-discharge capacity curves for low and high sweep rates are shown in Fig. 8(c).

At the slower sweep rate (0.5 mV/s), the discharge and charge capacities started with higher values and decreased due to the particle size effect. As mentioned in the previous section, the conversion reactions during Li$^+$ insertion/de-insertion produce homogeneous nanoparticles of $Cu_2O$, Cu and $Li_2O$ however, due to the higher quantity of $Cu_2O$ a large numbers of cycles (first 20 cycles) are required to achieve uniform particles size. Once the particles size are consistent, the discharge-charge capacity increases and stabilises

10

from 31$^{st}$ cycle forwards with slightly higher capacity (401 mAhg$^{-1}$) than that recorded for the earlier sample with thin oxide outside the Cu support. The higher specific capacity may be attributed to the presence of a large amount of Cu nanodomains during the charging process which form an interconnected network between Li$_2$O particles and could thereby enhance the reactivity of Li$_2$O reconversion to Cu$_2$O due to the high surface activity as well as electronic conductivity in the recharging process [5, 14].

When the same Cu$_2$O nanotubes are cycled at 5 and 2 mV/s each for 20 consecutive cycles (Fig. 7(b)) the initial capacity (388 mAhg$^{-1}$) for both cases is consistent with the above observation for the slower sweep rate (Fig. 8(c)). The slight decrease in Li$^+$ storage capacity of Cu$_2$O nanotubes may be indicative of the lower Li$^+$ insertion/de-insertion rates in the same potential intervals at higher sweep rates. The rate capability performance of Cu$_2$O nanotubes measured after 80 cyclic voltammograms as described above and cycles at three current densities of 1.67 mA/cm$^2$, 3.33 mA/cm$^2$ and 5 mA/cm$^2$ are shown in Fig. 9(a - c). There are three clear potential ranges at 3.0 - 1.75 V, 1.25 – 0.35 V and 0.35 – 0 V in the curves as shown in Fig. 9(a) and (b) consistent with three cathodic peaks in the cyclic voltammograms. The discharge-charge plateau appears as a smooth shoulder at the current density of 5 mA/cm$^2$ (Fig. 9(c)). The specific capacities at 1.677 mA/cm$^2$ (455 mAhg$^{-1}$), 3.33 mA/cm$^2$ (450 mAhg$^{-1}$) and 5 mA/cm$^2$ (440 mAhg$^{-1}$) are quite similar for each of the current densities investigated. Therefore it is clear that the rate capability perforamance of Cu$_2$O nanotubes can be as high as 5 mA/cm$^2$ with little decrease in the available capacity of the core/shell electrode material.

Subsequently, the same Cu$_2$O electrode was cycled at constant current density of 1.67 mA/cm$^2$ and a time limited total charge-discharge of 1 hour. Fig. 10 shows the last 11

discharge-charge curves started from 84th cycle. It can be seen from the graph that initially the discharge-charge curve reaches a potential minimum of 0 V but in later cycles reversed at approximately 0.65 V vs. Li/Li$^+$. Initially the limited time was sufficient to utlise the full Li storage capacity (455 mAhg$^{-1}$) of the $Cu_2O$ nanotubes. However, utilisation of additional capacity generated over cycling by the $Cu_2O$ electrode required a longer cycle time. Therefore, the lower potential limit achieved during discharge shifts to the more positive potential with cycling. The cycling performances of $Cu_2O$ nanotubes shows a high level of structural integrity as capacity was retained even after 94 cycles when cycled at 1.67 mA/cm$^2$. The structural integrity and consequnt long cycleability is also supported by SEM images taken after Li cycling, see Fig. 11(a and b). The $Cu_2O$ nanotubes remained free standing on the substrate with uniform nanosized particles formed with cycling. The observed SEM images are consistent with the explanations given earlier for the higher capacity of $Cu_2O$ nanotubes in terms of homogeneous nanoparticles size effects during the conversion reactions.

To explain the enhanced cyclability of the structures reported in this work two types of $Cu_2O$ nanotubes must be considered. We studied $Cu_2O$ nanotubes (i) with no metallic Cu, and (ii) with metallic Cu as inner support. When Cu nanotubes are fully converted to $Cu_2O$ very low cycleability is observed. After 20 cycles (at 0.5 mV/s vs Li) the retention capacity is reduced to 10% of the initial value, see Fig. 12.

To explain the electron-conducting mechanism and structural integrity of $Cu_2O$ nanotubes we propose the following, see Fig. 13. In the case of the $Cu_2O$ nanotubes with metallic Cu as the inner core support with high electrical conductivity, Fig. 13(a), the reaction commences along the full length of the nanotube walls and structural and

electrical integrity is maintained in this core(metal)/shell(oxide) type structure upon $Li^+$ insertion, Fig 13(b), and extraction Fig 13(c).

For fully converetd $Cu_2O$ nanotubes Fig 13(d), the conversion reaction starts at the base connection with the substrate and then gradually propagates through the nanotubes. Fig 13 (e) is representative of a point close to the base of the nanotube where all of the $Cu_2O$ converts to Cu and $Li_2O$. Further up the nanotube not all of the tube will convert as the electrical conductivity of the $Cu_2O$ will not support a relatively high reaction and conversion rate. On the subsequent $Li^+$ extraction less Li will be removed as the nanoscale particles of Cu will not have sufficient interconnectivity to facilitate the conversion reaction, Fig 13(f). Again this reaction will be exacerbated further up the 20 μm long nanotubes. This leads to the poor cycliability recorded in Fig. 12 for the substrate where all of the Cu core was oxidised to $Cu_2O$ prior to lithium test.

**Conclusion**

A direct electrodeposition technique for high quality Cu nanotube arrays and subsequent conversion of the deposited Cu into $Cu_2O$ has been developed. The $Cu_2O$ nanotube arrays have shown high capacity, cycleability and rate capability. The cycling performance of $Cu_2O$ nanotubes shows a high level of structural integrity with capacity retention even after 94 cycles when cycled at 1.67 mA/cm$^2$ (approximately 1C rate). The electrochemical performance of the $Cu_2O$ nanotubes is enhanced by the high surface area, easy infiltration of electrolytes, high electrical conductivity of Cu support and structural integrity. The $Cu_2O$ nanotubes also eliminate the requirment of ancillary materials typically used in Li-ion batteries, such as carbon particles to increase conductivity.

## Acknowledgments

## References

1.  C. R. Sides and C. R. Martin, *Nanomaterials in Li-ion battery electrode design, Modern aspects of Electrochemistry*, No. 40, R. E. White Editor, 75, Springer, New York  (2007).

2.  N. Li, C.R. Martin and B. Scrosati, *J. Power Sources.* **97**, 933 (2001).

3.  Y. Wang and G. Cao, *Adv. Mater.*, **20**, 2251 (2008).

4.  J. H. Kim, S. Khanal, M. Islam, A. Khatri and D. Choi, *Electrochem. Commun.*, **10**, 1668 (2008).

5.  P. Poizot, S. Laruelle, S. Grugeon, L. Dupont and J.-M. Tarascon, *Nature*, **407**, 496 (2000).

6.  P.L. Taberna, S. Mitra, P. Poizot, P. Simon and J.-M. Tarascon, *Nat. Mater.*, **5**, 567 (2006).

7.  Y. Li, B. Tan and Y. Wu, *Nano Lett.*, **8**, 265 (2008).

8.  S. Grugeon, S. Laruelle, R.H Urbina, L. Dupont, P. Poizot and J.-M. Tarascon, *J. Electrochem. Soc.*, **148**, A285 (2001).

9.  R. Inguanta, S. Piazza and C. Sunseri, *Electrochim. Acta*, **53**, 6504 (2008).

10. S. Wang, Q. Huang, X. Wen, X-Y. Li and S. Yang, *Phys. Chem. Chem. Phys.*, **4**, 3425 (2002).

11. A. M. Hermann, P. A. Ramkrishnan, V. Badri, P. Mardilovich and W. Landuyt, *Int. J. Hydrogen Energy*, **26**, 1295 (2001).

12. C. Mu, Y. Yu, R. Wang, K. Wu, D. Xu and G. Guo, *Adv. Mater.*, **16**, 1550 (2004).

13. T. Chowdhury, D.P. Casey and J.F. Rohan, *Electrochem. Commun.*, **11**, 1203 (2009).

14. Y.H. Lee, I.C. Leu, S.T. Chang, C.L. Liao and K.Z. Fung. *Electrochim. Acta*, **50**, 553 (2004).

15. C.Q. Zhang, J.P. Tu, X.H. Huang, Y.F. Yuan, X.T. Chen and F. Mao, *J. Alloy Compd.*, **441**, 52 (2007).

16. L.Y. Beaulieu, S.D. Beattie, T.D. Hatchard and J.R. Dahn*, J. Electrochem. Soc.*, **150,** A419 (2003).

17. N. Pereira, L.C. Klein and G.G. Amatucci, *Solid Sate Ionics*, **167**, 29 (2004).

18. H.-C. Shin and M. Liu, *Adv. Funct. Mater*, **15**, 582 (2005).

19. M. Inaba, T. Uno and A. Tasaka, *J. Power Sources*, **146,** 473 (2005).

**Figures.**
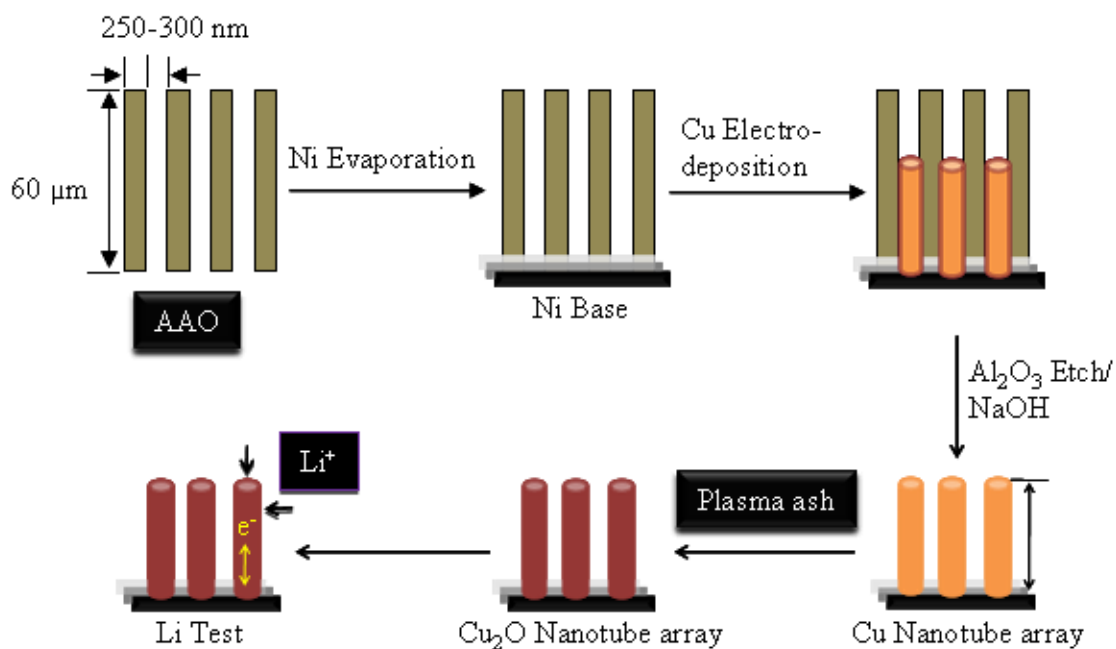


Figure 1. Schematic illustration of the synthesis process for high aspect ratio Cu₂O nanotube arrays.
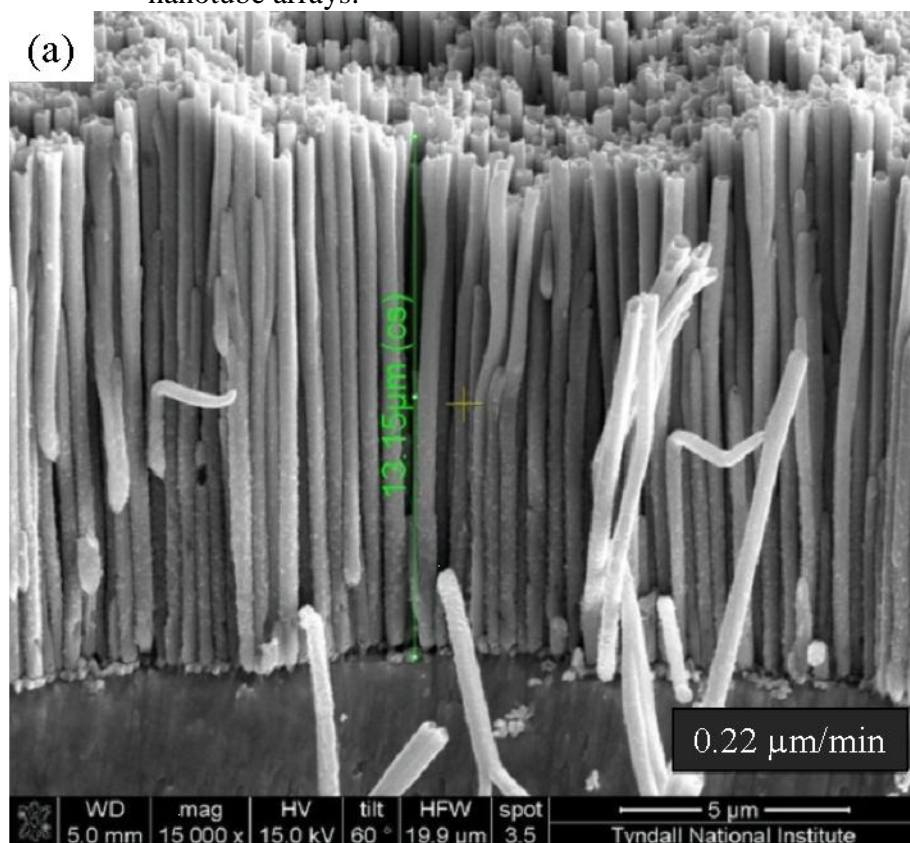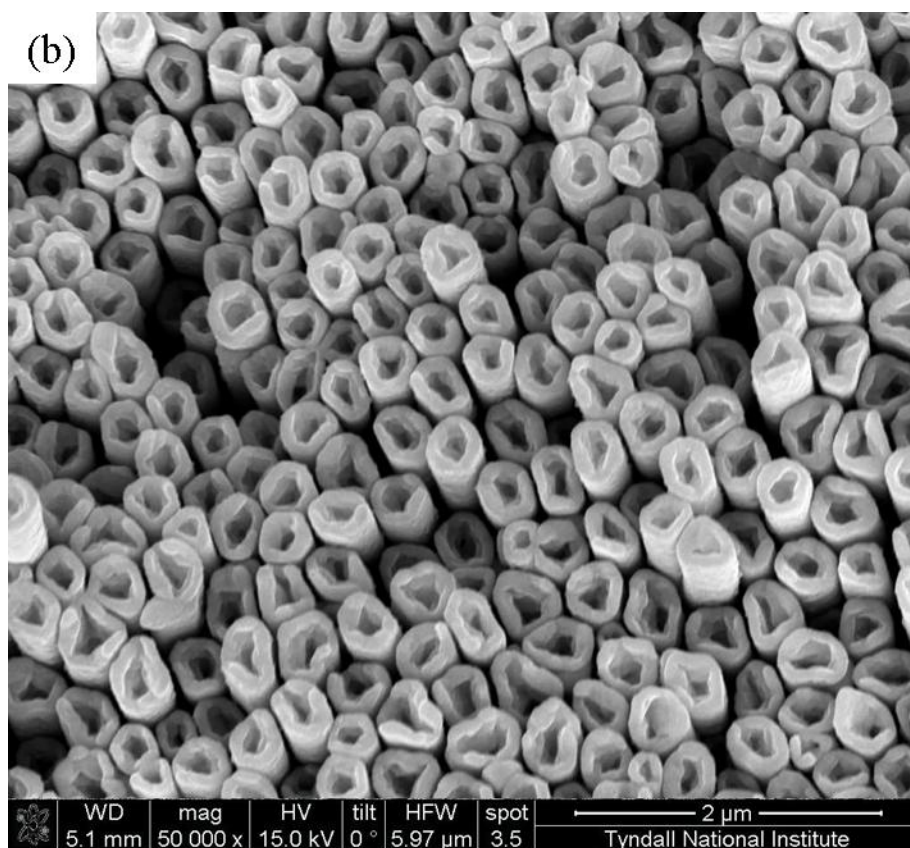
Figure 2.    SEM images of as-synthesised Cu nanotube arrays,  (a) cross-sectional and (b) plan view.
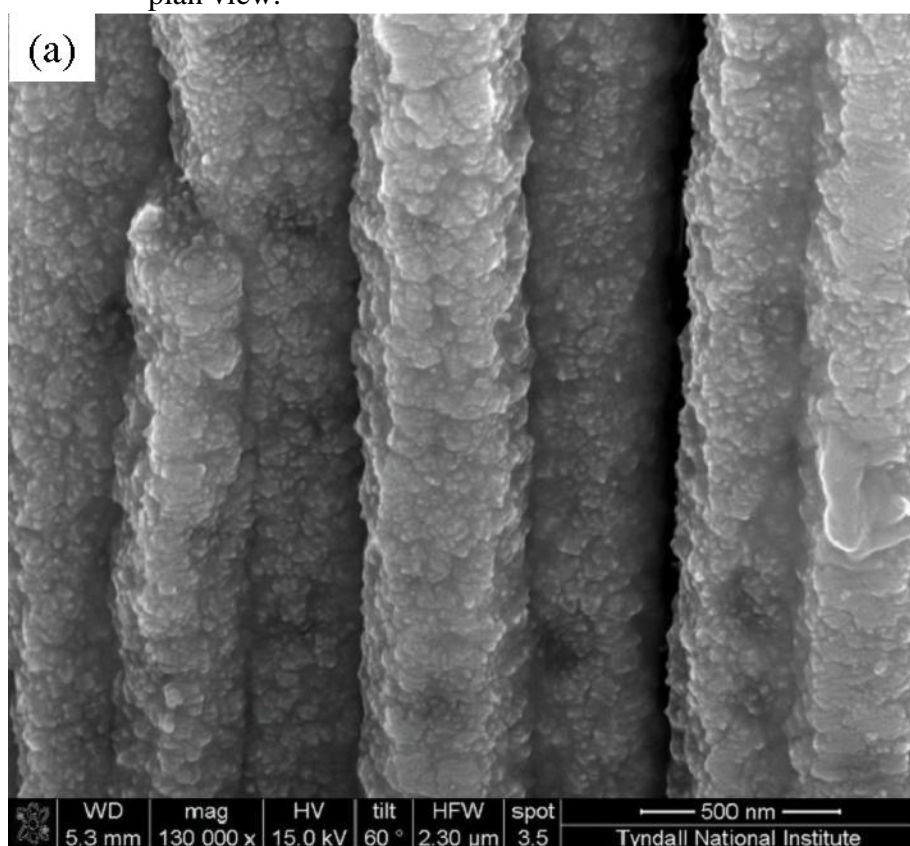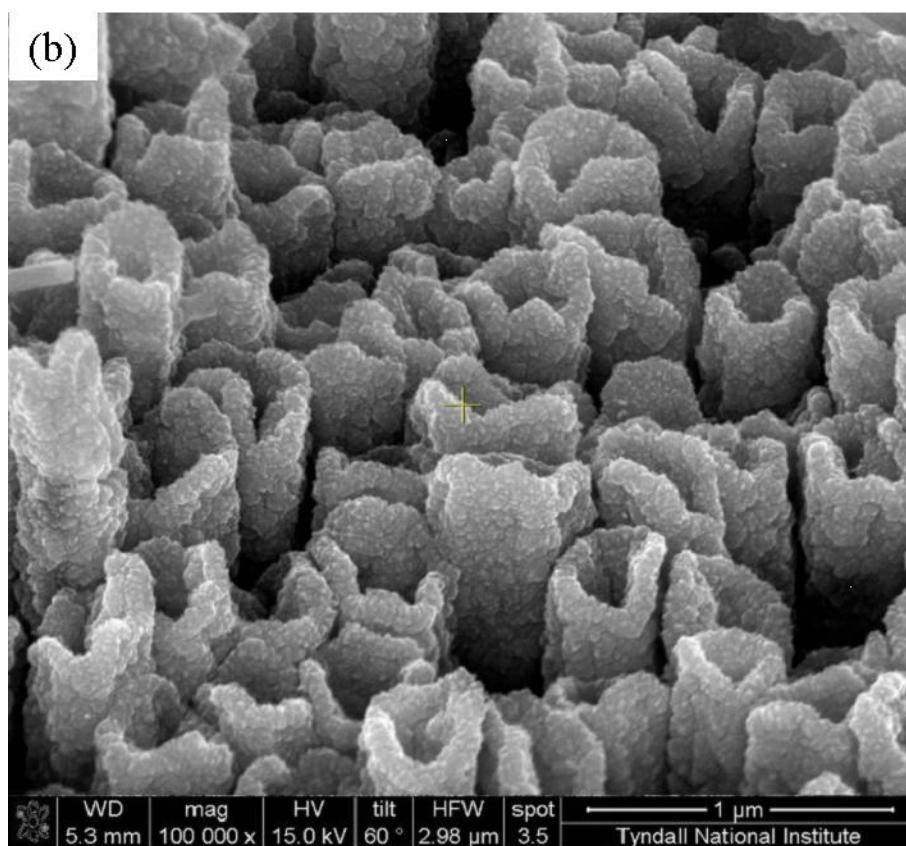
Figure 3.   SEM images of the Cu$_2$O nanotube arrays obtained from Cu nanotubes after oxygen plasma treatment for 4.5 minutes, (a) cross-sectional and b) plan view.
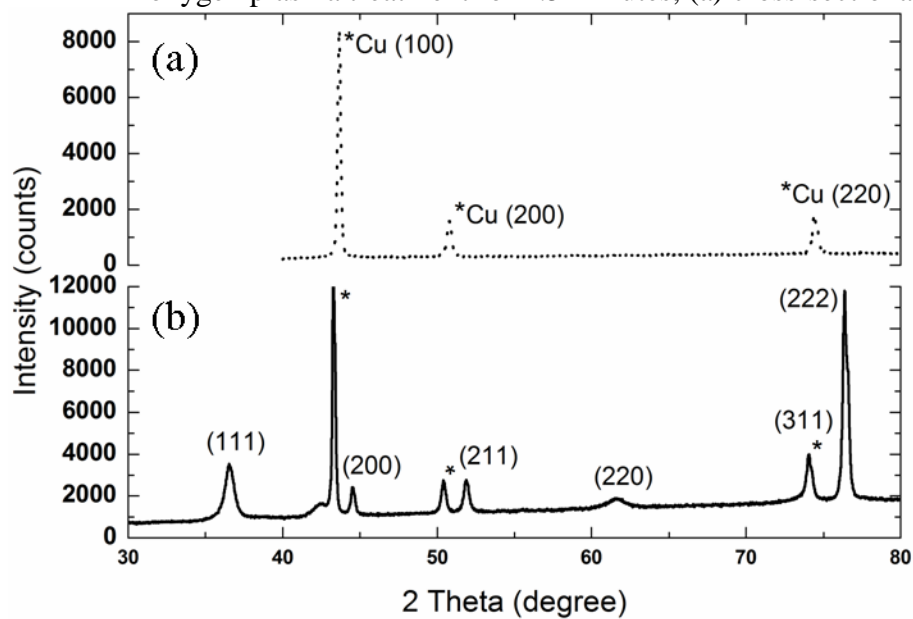


Figure 4.   XRD patterns of (a) Cu nanotubes after removal of the AAO template and (b) Cu$_2$O nanotubes (oxygen plasma treatment 4.5 minutes).
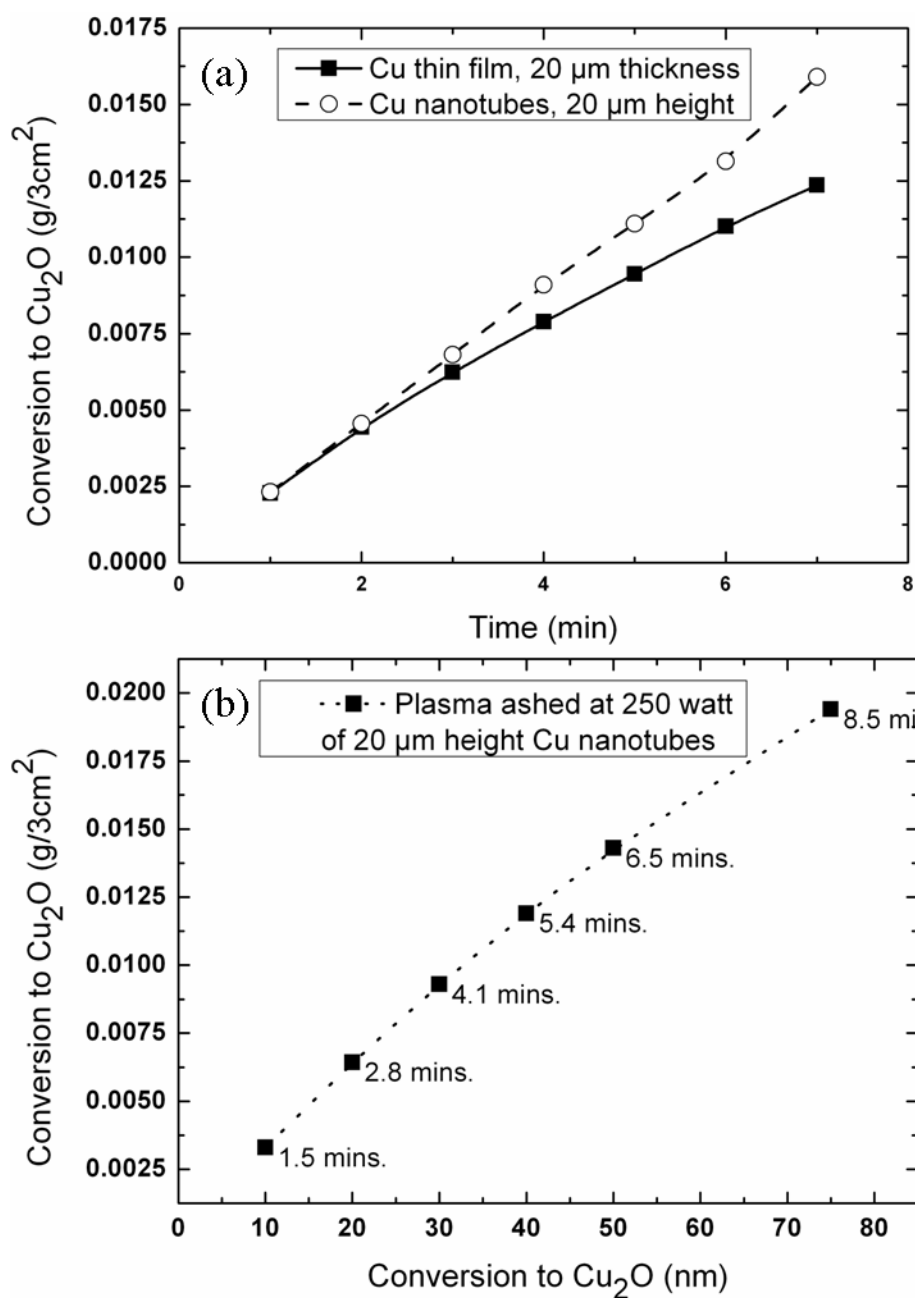
Figure 5.   Conversion rate plots for Cu to Cu$_2$O by oxygen plasma treatment, (a) time related plot and (b) correlation plot for a series of oxygen plasma times.

(a)

| HV | WD | HFW | mag | spot | 2/3/2010 | ⊢— 500 nm —⊣ |
|---|---|---|---|---|---|---|
| 5.00 kV | 12.3 mm | 2.30 µm | 130 000 x | 2.5 | 2:53:58 PM | |

(b)

| HV | WD | HFW | mag | spot | 2/3/2010 | ⊢— 500 nm —⊣ |
|---|---|---|---|---|---|---|
| 5.00 kV | 12.1 mm | 2.30 µm | 129 993 x | 2.5 | 3:01:08 PM | |

21
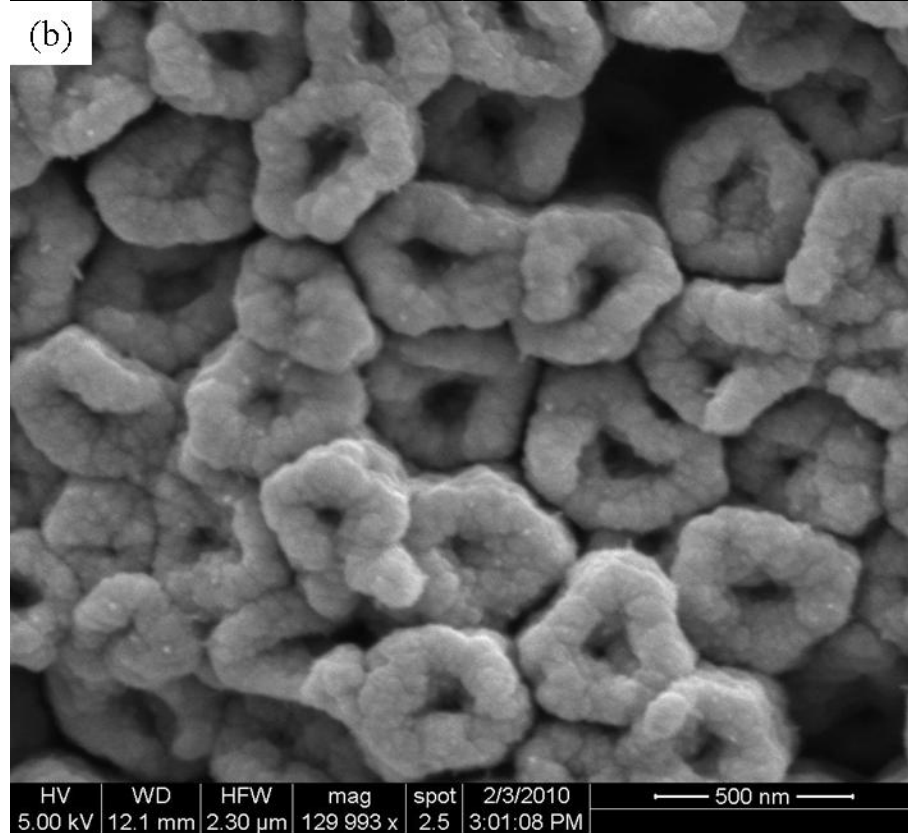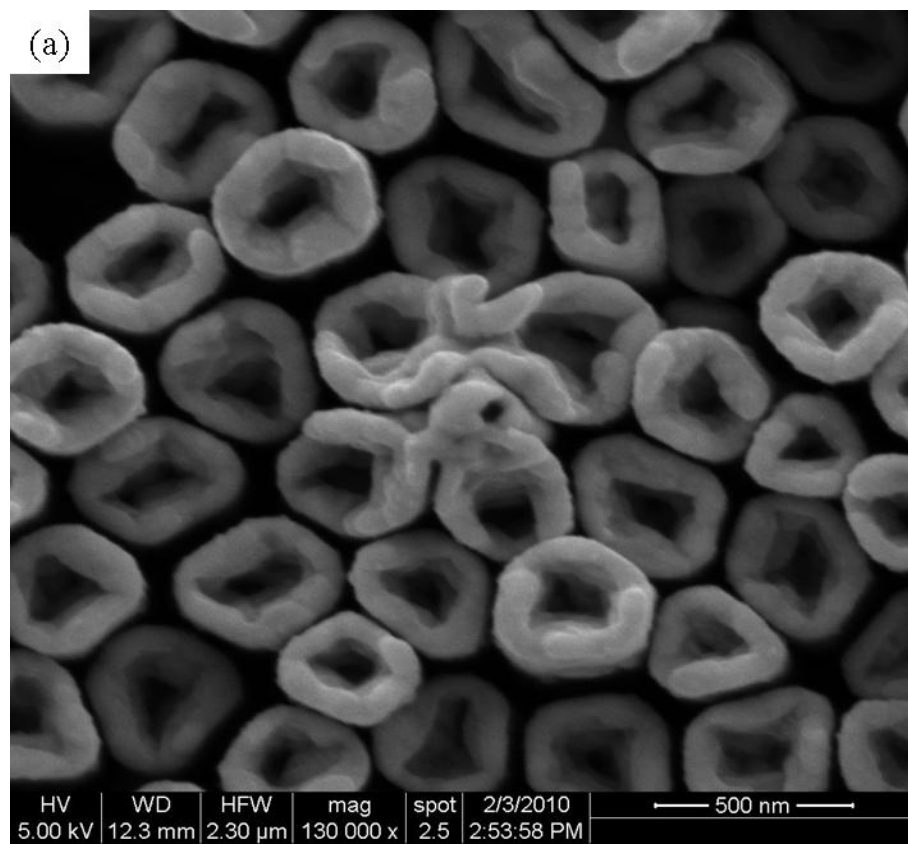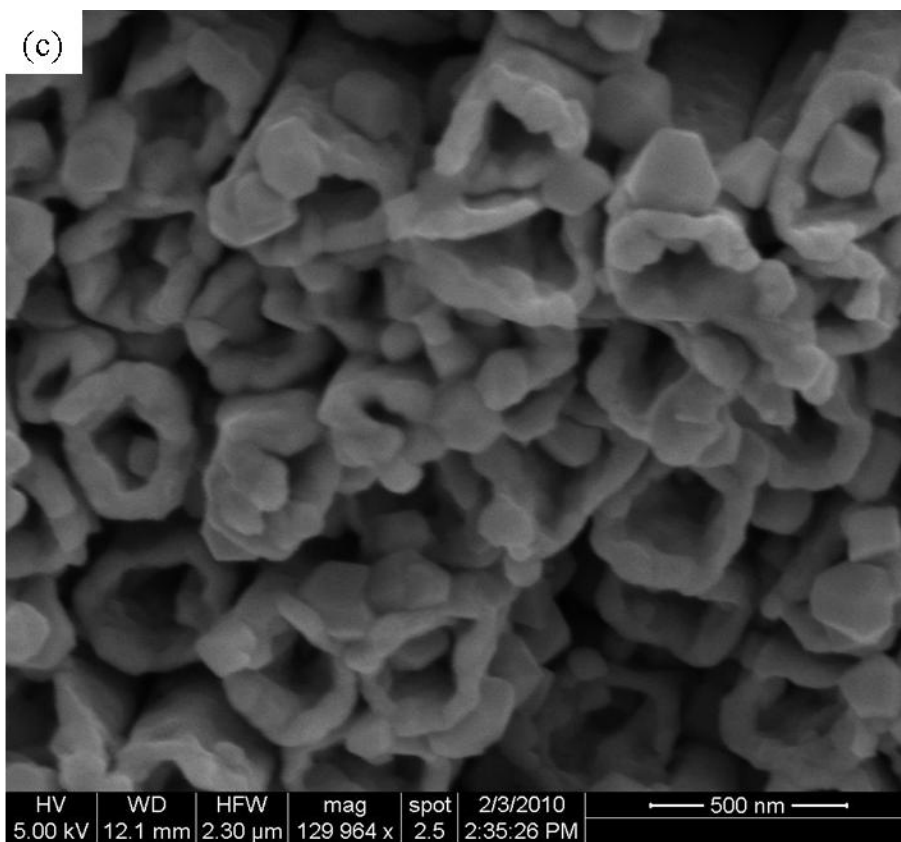
Figure.6    SEM image of (a) Cu nanotubes, (b) $Cu_2O$ nanotubes (oxygen plasma treatment for 4.1 mins) and (c) Thinned Cu metal core support after oxide removal by Schloetter S20 (sulphuric acid based) solution.
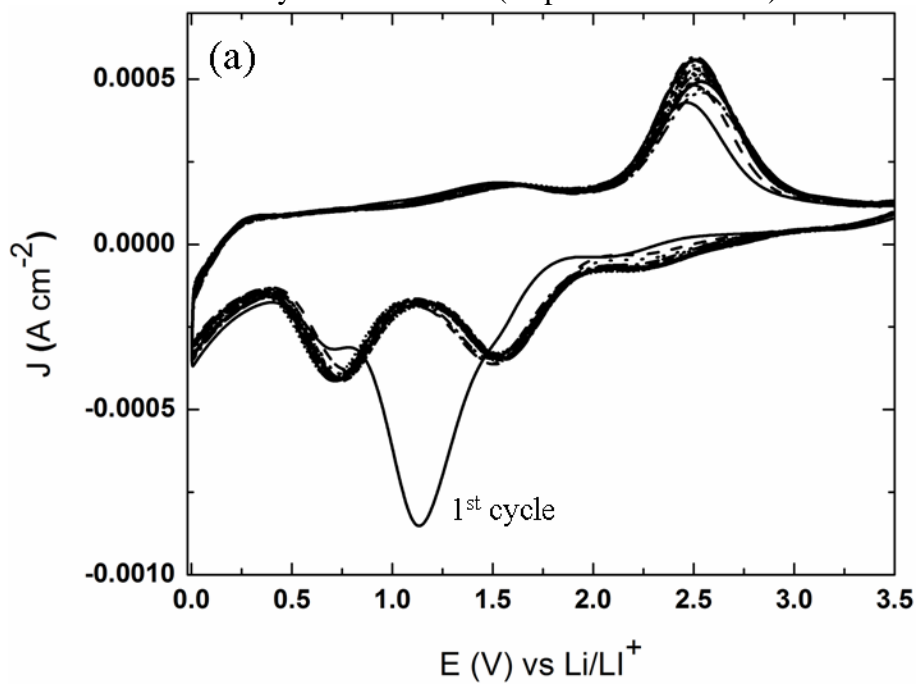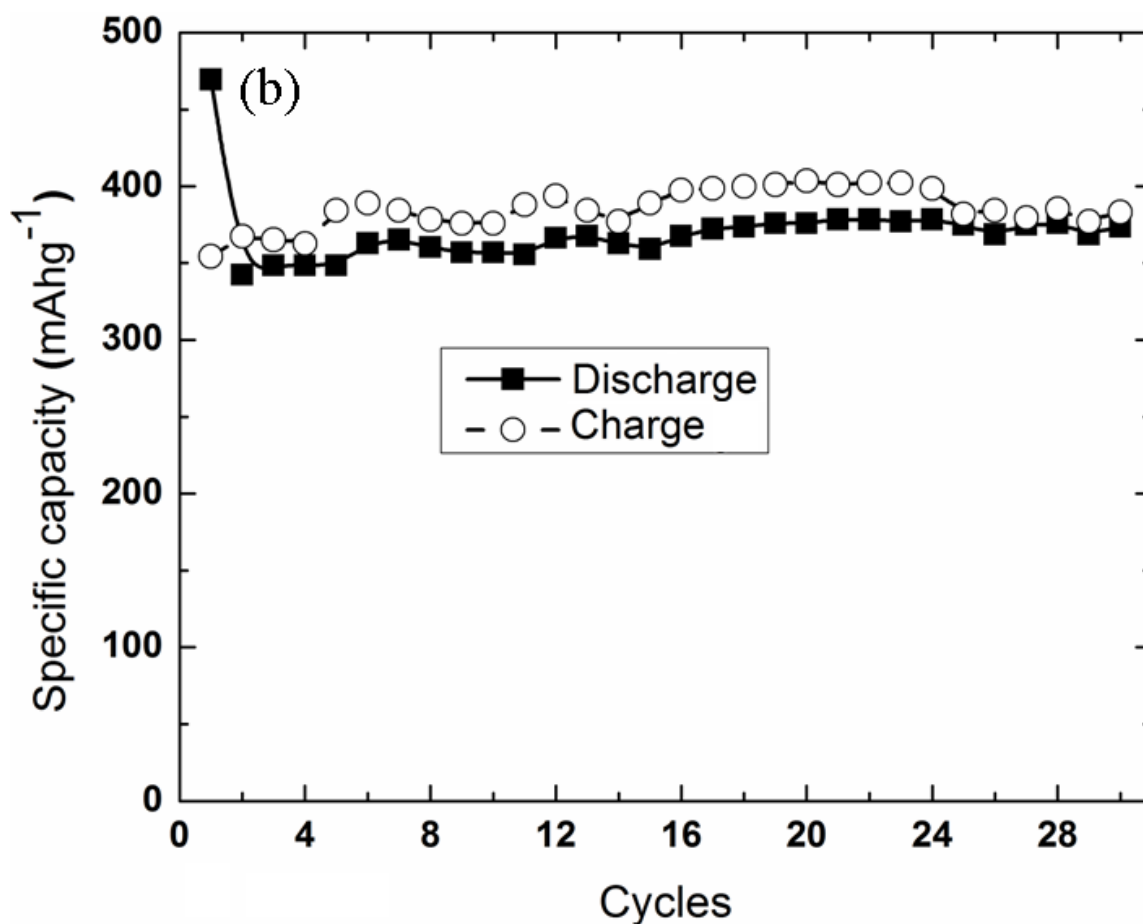
Figure 7. (a) First 20 cyclic voltammograms of Cu$_2$O nanotubes (oxygen plasma treatment for 1 min) Sweep rate 0.5 mV/s, and (b) Discharge-charge capacity vs. cycle number for 30 cycles of the Cu$_2$O nanotubes.
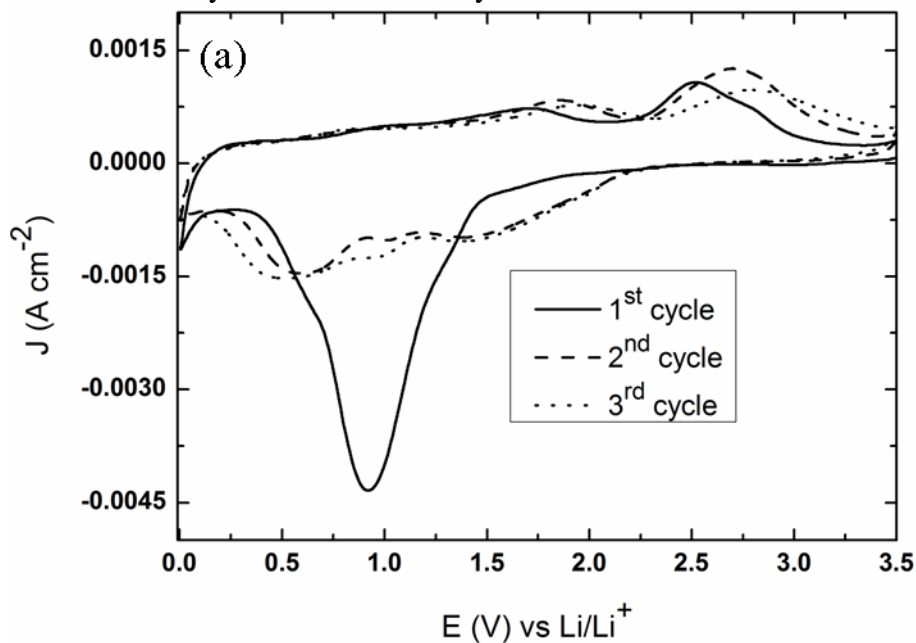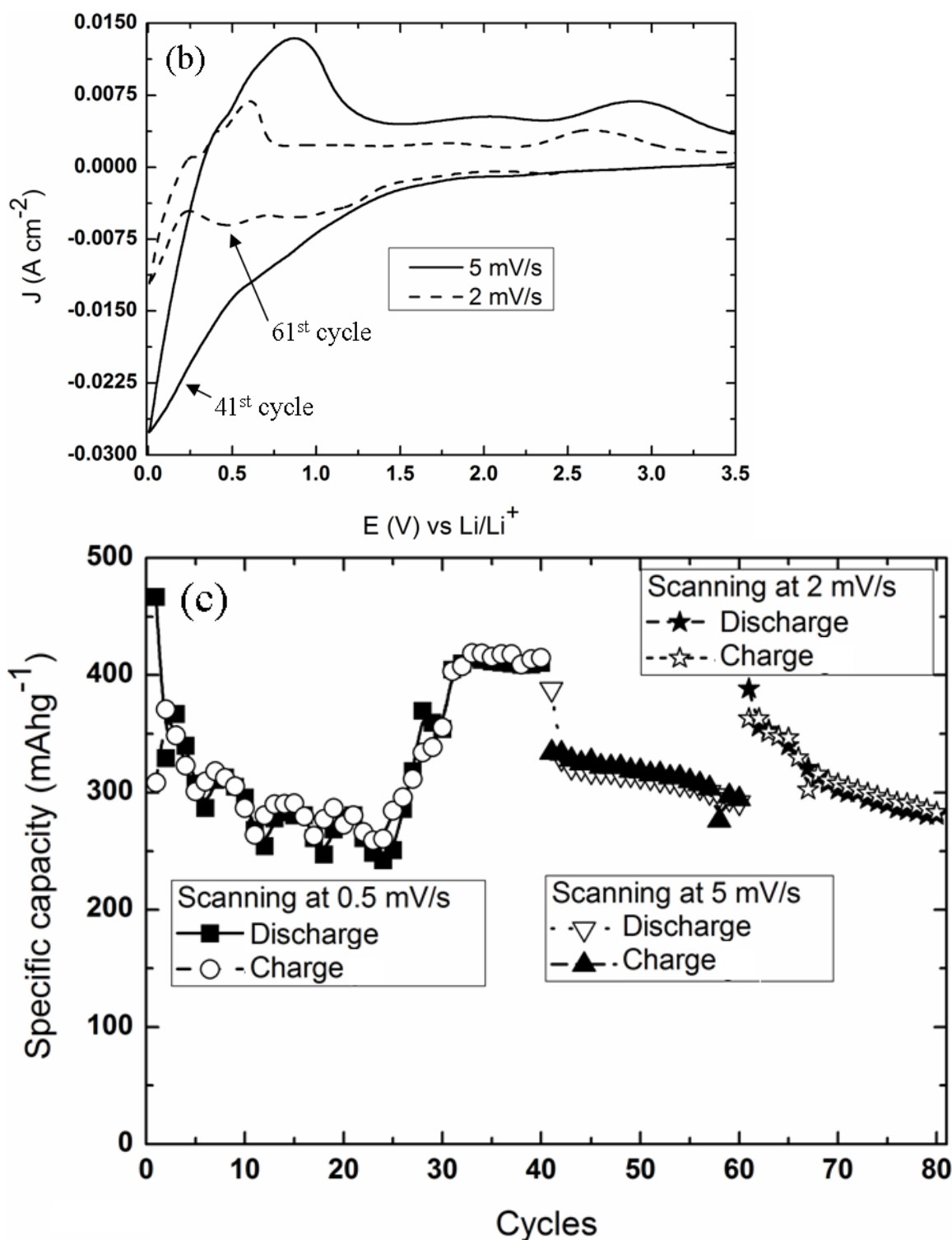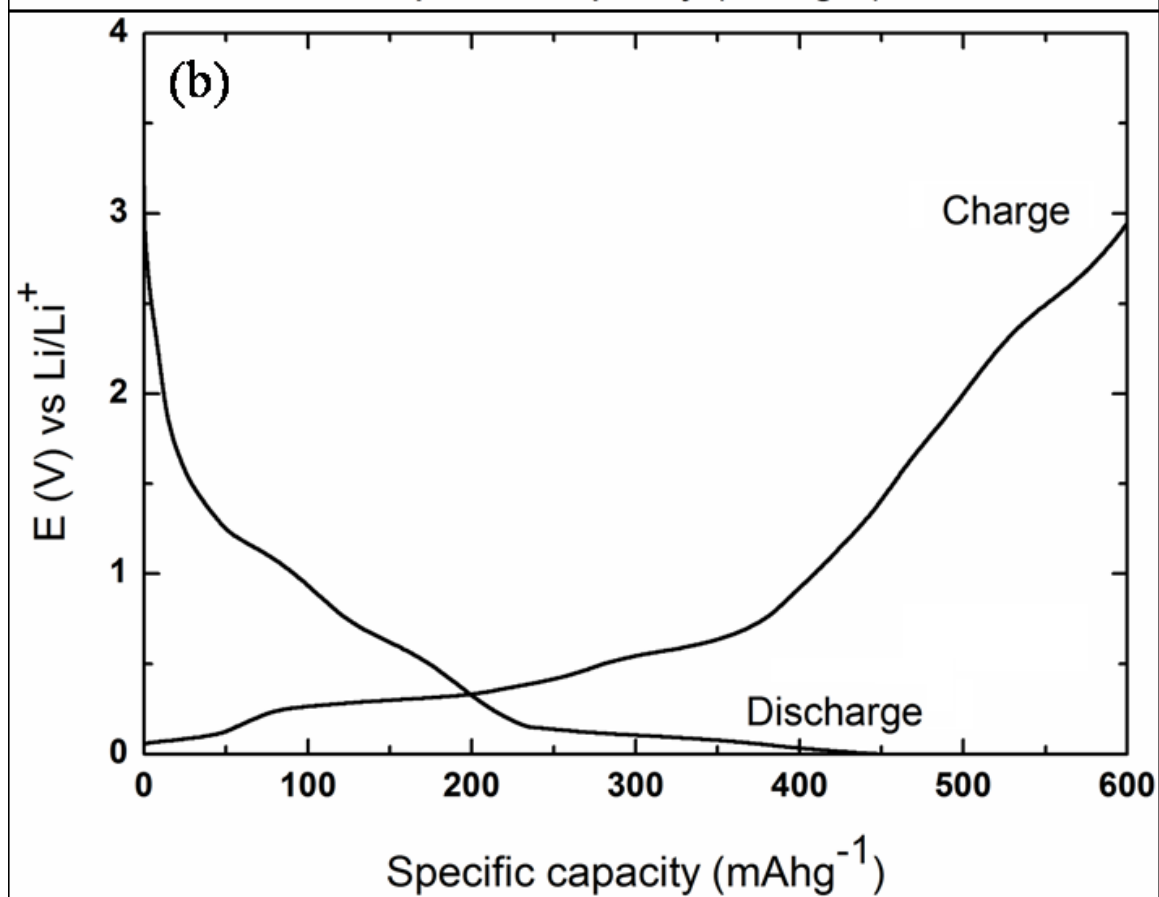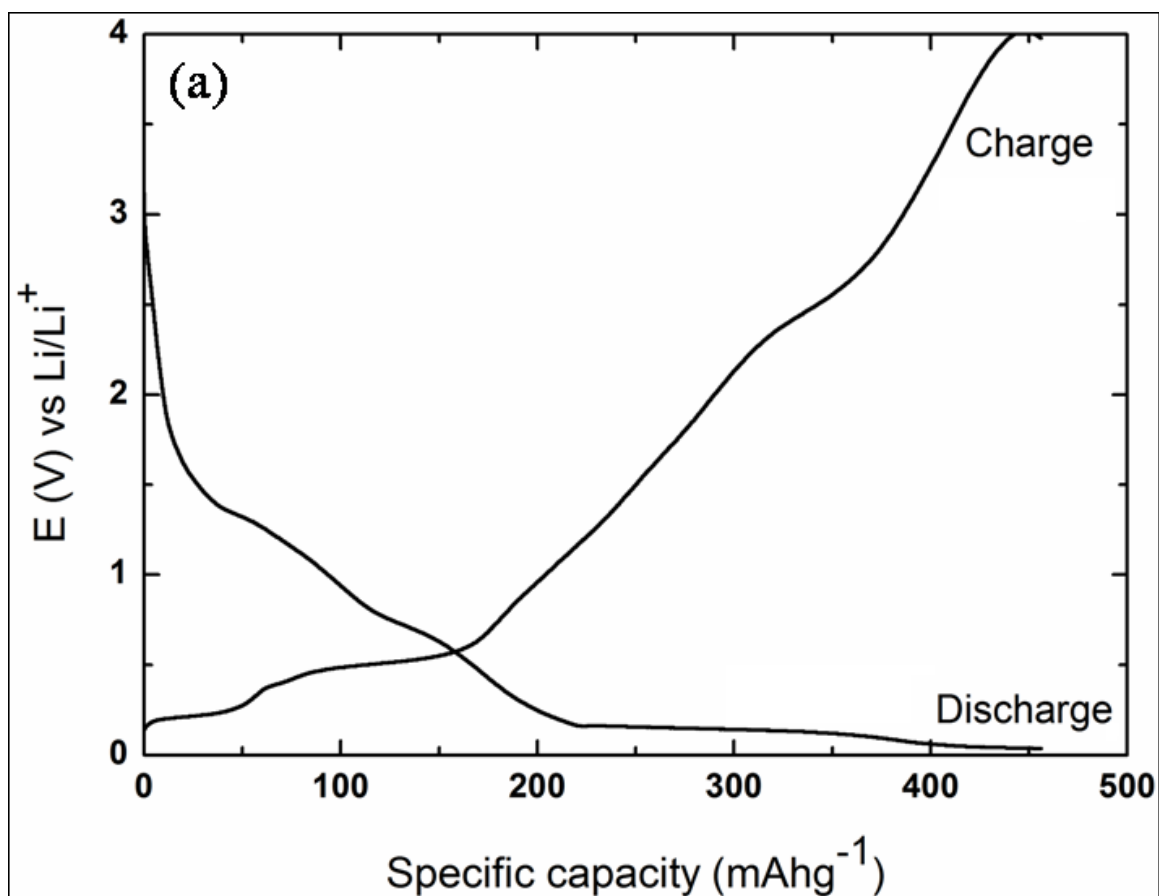
Figure 8. (a) First 3 cyclic voltammograms of $Cu_2O$ nanotubes (oxygen plasma treatment for 4.5 min). Sweep rate 0.5 mV/s, (b) 41st and 61st cyclic voltammograms of $Cu_2O$ nanotubes with sweep rate of 5 mV/s and 2 mV/s, respectively, (c) Discharge-charge capacity vs. cycle number curves of $Cu_2O$ nanotubes for 80 cycles at various sweep rates.
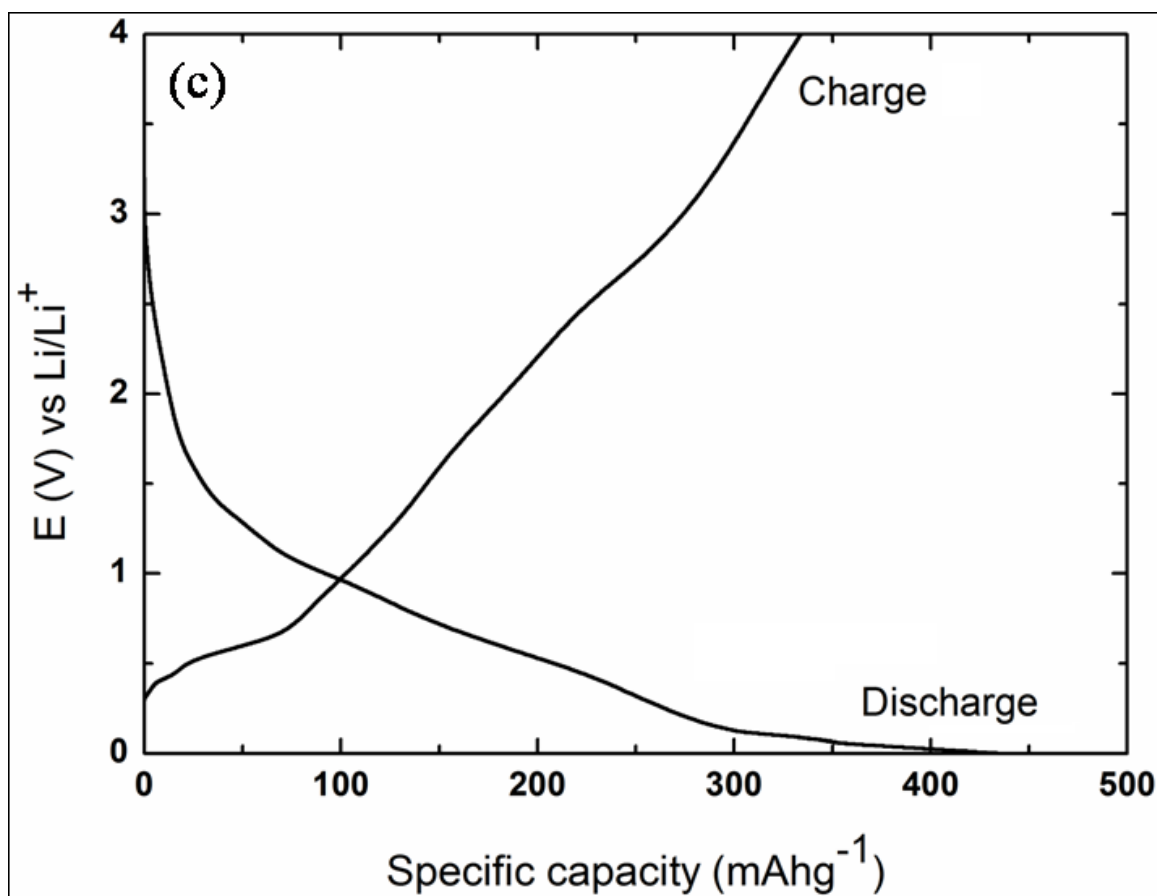
Figure 9. Discharge-charge curves of $Cu_2O$ nanotubes from the 81st cycle at current densities of (a) 1.67 mA/cm$^2$, (b) 3.33 mA/cm$^2$ and (c) 5 mA/cm$^2$.
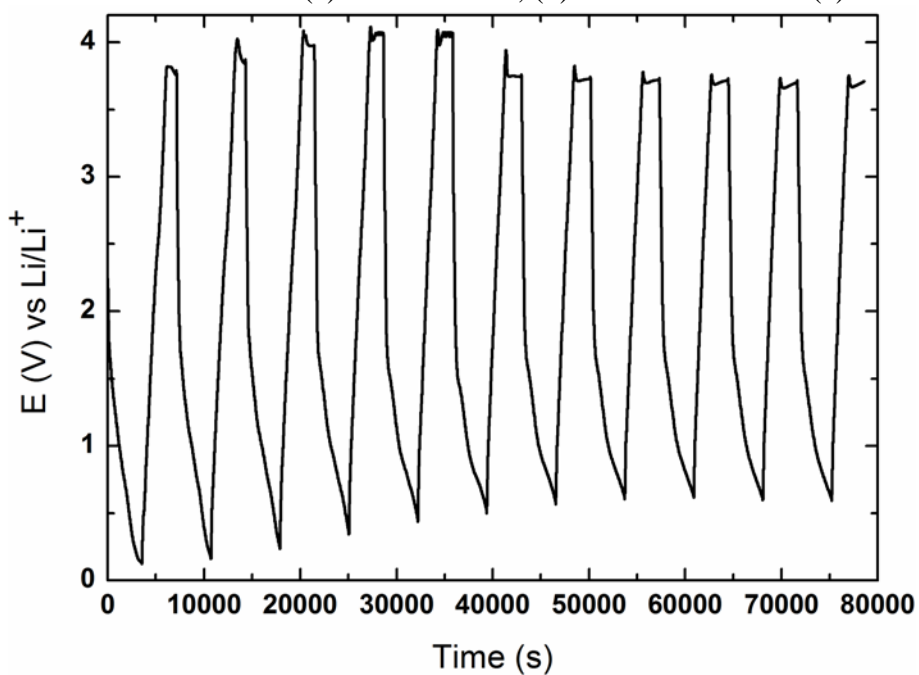


Figure 10. Discharge-charge curves of $Cu_2O$ nanotubes from 84th cycle at current density of 1.67 mA/cm$^2$ for 11 cycles.
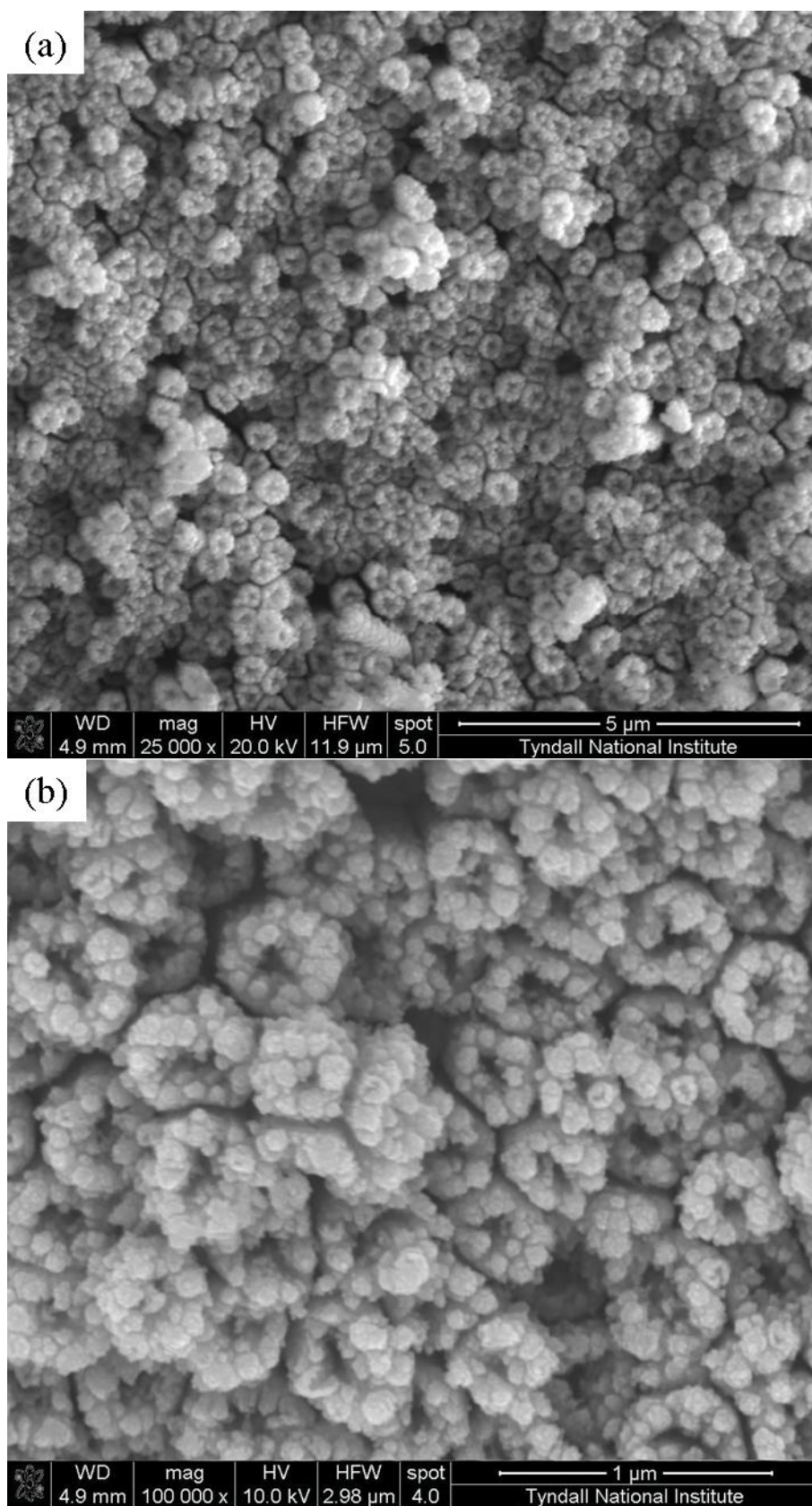
(a)

| WD | mag | HV | HFW | spot | 5 μm |
|---|---|---|---|---|---|
| 4.9 mm | 25 000 x | 20.0 kV | 11.9 μm | 5.0 | Tyndall National Institute |

(b)

| WD | mag | HV | HFW | spot | 1 μm |
|---|---|---|---|---|---|
| 4.9 mm | 100 000 x | 10.0 kV | 2.98 μm | 4.0 | Tyndall National Institute |

Figure 11. SEM images of $Cu_2O$ nanotubes after 94 cycles, (a) plan view, magnification x25,000 and (b) plan view, high magnification x100,000.
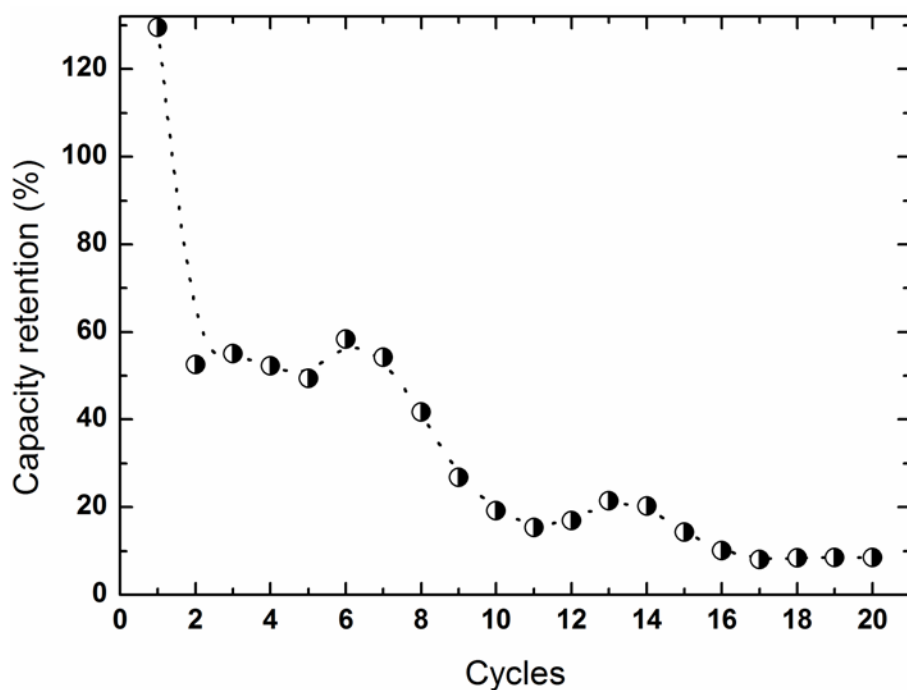
Figure 12. Capacity retention vs cycle number curve of $Cu_2O$ nanotubes (fully converted) with sweep rate of 0.5 mV/s.
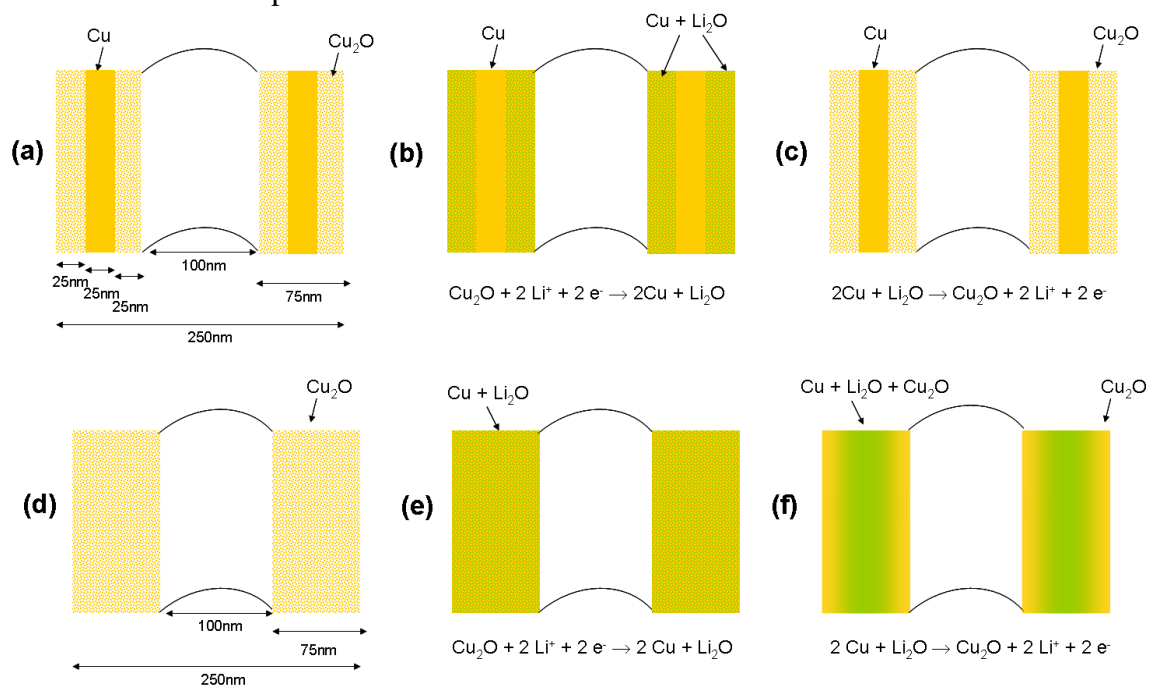


Figure 13. Schematic illustration of the electrochemical conversion reaction of $Cu_2O$ nanotubes (a) $Cu_2O$ outside a Cu core prior to $Li^+$ insertion, (b) Cu and $Li_2O$ outside Cu core after $Li^+$ insertion, (c) Restored $Cu_2O$ outside a Cu core after $Li^+$ extraction, (d) $Cu_2O$ nanotubes without metallic Cu core, (e) Cu and $Li_2O$ after $Li^+$ insertion, (f) $Cu_2O$ outside isolated $Li_2O$ and discontinuous Cu which cannot support the extraction mechanism due to loss of electrical contact.